

ARTICLE OPEN



Physics-based electrical modelling of CIGS thin-film photovoltaic modules for system-level energy yield simulations

Santhosh Ramesh^{1,2,3,4}✉, Arttu Tuomiranta^{1,2,4}, Ali Hajjiah⁵, Marc Meuris^{1,2,4}, Bart Vermang^{1,2,4} and Jef Poortmans^{1,2,3,4}

Copper indium gallium selenide (CIGS) is a commercialized, high-efficiency thin-film photovoltaic (PV) technology. The state-of-the-art energy yield models for this technology have a significant normalized root mean square error (nRMSE) on power estimation: De Soto model—26.7%; PVsyst model—12%. In this work, we propose a physics-based electrical model for CIGS technology which can be used for system-level energy yield simulations by people across the PV value chain. The model was developed by considering models of significant electrical current pathways from literature and adapting it for the system-level simulation. We improved it further by incorporating temperature and irradiance dependence of parameters through characterisation at various operating conditions. We also devised a module level, non-destructive characterization strategy based on readily available measurement equipment to obtain the model parameters. The model was validated using the measurements from multiple commercial modules and has a significantly lower power estimation nRMSE of 1.2%.

npj Flexible Electronics (2022)6:87; <https://doi.org/10.1038/s41528-022-00220-5>

INTRODUCTION

Photovoltaics has evolved from an additional power source in small calculators to a clean energy source in mainstream energy production. The growing concerns over climate change have fuelled further evolution towards innovative concepts like vehicle-integrated PV, net-zero energy buildings and net-zero energy districts. In many of these applications, thin-film PV technologies are more suitable than crystalline silicon (c-Si) solar cells. The thin-film technologies have existed for decades, but c-Si PV has dominated the PV industry with its high efficiency, stability, and mature manufacturing processes¹. The thin-film PV technologies are known for their aesthetic appeal and the possibility to fabricate them on flexible substrates. With such characteristics, thin-film PV technologies may gain market share in the domain of integrated photovoltaics (IPV). A report by Becquerel Institute² states that, in 2020, the European IPV market was valued at almost 600 million euros and projected to triple reaching 1800 million euros by 2023. The case study in the report highlights the cost-effectiveness of thin-film technologies. The report also identifies digitization as one of the major factors needed to boost the economy around IPV. A modelling infrastructure for reliable energy yield prediction is a step in that direction as it assists in developing and optimizing thin-film PV systems for maximum energy yield. In this work, we focus on creating an energy yield model for system-level simulation for the CIGS technology.

CIGS solar cells have additional current mechanisms that make the current–voltage (*IV*) characteristics unique compared to conventional solar cells. In c-Si solar cells, the current–voltage (*IV*) characteristics can be constructed by super positioning the dark behaviour and the photogenerated current at short circuit. This superposition fails in CIGS solar cells because of the voltage-dependent photogeneration^{3–5}. This can be seen in the measured dark and illuminated *IV* curves shown in Fig. 1. The current mechanisms that contribute to the photocurrent in CIGS solar cells are drift current across the depletion region to the heterojunction

interface, thermionic emission across the junction, bulk recombination, and diffusion to the back contact. The voltage dependence is caused by the drift and the thermionic emission losses that are linked to the change in the electric field and increased back contact recombination^{6–8}. The electric field and the depletion layer width, in turn, are voltage dependent. The parasitic currents in CIGS solar cells are junction recombination current, ohmic shunt current, space charge limited current (SCLC), and tunnelling currents⁹. The recombination current in CIGS solar cells varies with illumination as some defects are activated upon illumination^{10,11}. Shunt current is related to the presence of pinholes in the absorber. The absence of buffer and window layers results in a local metal-semiconductor-metal contact which leads to SCLC^{12–15}. The tunnelling currents are caused by mid-gap defects that are significant at temperatures below 250 K¹¹ and can be ignored for the energy yield estimation.

One of the commonly used models for PV module performance is the *Sandia PV Array Performance Model* (SAPM)¹⁶. This model uses *IV* characteristics to estimate fitting coefficients to represent the relation of the *IV* parameters at different operating conditions. This model was first developed for c-Si modules but has also been used for thin-film modules based on CIGS and cadmium telluride (CdTe) technologies^{17,18}. A database of the fitting coefficients for different modules is publicly available and integrated into open-source software packages such as System Advisory Model (SAM)¹⁹ and pvlb²⁰, and commercial software like PVsyst²¹. The *Loss Factor Model* (LFM)²² like SAPM, uses the outdoor measurement data to obtain a set of coefficients to correct temperature and spectral mismatch. LFM and SAPM are both empirical models. These models require a significant amount of onsite measurement data to calibrate the parameters for realistic energy yield estimation.

Physics-based models consider the variation of the physical parameters with the external operating conditions to simulate the performance of solar cells. The availability of such models is minimal. The De Soto model²³ (aka the five-parameter model) is a

¹Ibmc, imo-imomec, Thor Park 8320, 3600 Genk, Belgium. ²EnergyVille, imo-imomec, Thor Park 8320, 3600 Genk, Belgium. ³KU Leuven, Dept. of Electrical Engineering (ESAT), Leuven, Belgium. ⁴Hasselt University, imo-imomec, Martelarenlaan 42, 3500 Hasselt, Belgium. ⁵Kuwait University, Dept. of Electrical Engineering, College of Engineering and Petroleum, Kuwait, Kuwait. ✉email: santhosh.ramesh@ibmc.be

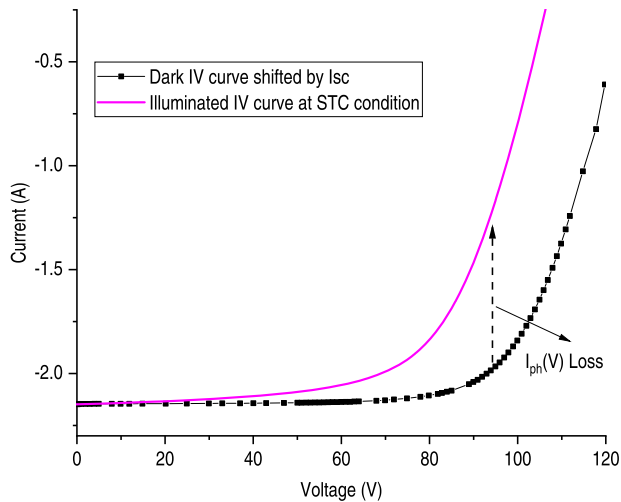


Fig. 1 Dark and illuminated *IV* superposition failure in a CIGS module. The illuminated *IV* (magenta) is measured at one sun and 25 °C. The dark *IV* (black) is measured at 25 °C and shifted by the I_{sc} value at one sun.

physics-based model based on the superposition of the dark and the illuminated *IV* curve of a solar cell. It has been widely used by the PV industry to represent the performance of the c-Si solar cells. PVsyst²¹ uses a modified version of the De Soto model where it considers an exponential relation between shunt and illumination intensity instead of a linear relation. The efficacy of De Soto and PVsyst models are tested and reported in the section “Statistical significance”. The analytical model described by Sun et al.⁶ is a physics-based model developed specifically for CIGS. It addresses the superposition failure by modelling the voltage dependence of photogeneration. However, this model does not consider the variation of saturation current and shunt resistance with illumination intensity, which are significant at low irradiance. The model was only validated at intensities above 400 W m^{-2} with laboratory-scale cells. The temperature and illumination dependence validated at the cell level may not be valid at the module level.

The reference parameters are parameters that represent the module characteristics at the Standard Test Conditions (STC). They are inputs to a model to estimate module performance at other operating conditions. Multiple techniques are available for estimating the value of such parameters. The nonlinear least-squares method is the most common technique to fit a model to data and obtain the parameters. It iteratively minimises the least square error. The requirement of initial values and bounded solution space for the parameters become a constraint for this method. Wrong initial estimates may lead to non-convergence or convergence to local minima. As the number of parameters increases, uncertainty in parameter estimation increases. This limits its use in large models. Another method is to reduce the number of model parameters by representing the possible dependent variables as a function of independent variables and iteratively solving the model to correctly estimate the power (P_{mpp}) at the maximum power point (MPP), the open-circuit voltage (V_{oc}) and the short-circuit current (I_{sc})²⁴. Both the above techniques are suitable for a simple model like the De Soto model.

The model described by Sun et al.⁶ has many parameters and they simplify the problem by individually fitting the current curves with their respective model i.e., fitting the reverse-biased dark current to their shunt current model, forward bias dark current to their diode current model. The photocurrent curve is obtained by separating the diode current and shunt current from the illuminated *IV* curve. Then, the photocurrent model is fitted to the photocurrent curve. For certain parameters, estimates were

obtained through the numerical simulation software ADEPT, which requires material-specific parameters (e.g., layer thickness, mobility, doping densities, and defects). This methodology by Sun et al. may be an interesting approach as it reduces uncertainty by splitting the model into three smaller parts. However, this strategy cannot be applied to parameterise the model for a commercial module. It is neither possible to measure the reverse-bias *IV* curve of commercial PV modules because of the presence of bypass diodes nor to have material-specific data like doping concentration, mobility, etc.

To set a benchmark, the accuracy of the existing state-of-the-art models to estimate the *IV* characteristics of CIGS modules were analysed. Although the CIGS-specific model with a parameter extraction methodology described by Sun et al.⁶ should be considered as the state of the art, it cannot be used at the module level. In this work, the variations of both De Soto and PVsyst models are considered as the state of the art for module-level simulations. The De Soto model is used along with the parameter extraction technique described by Laudani et al.²⁴. The performance estimation data of the PVsyst model was obtained from the module database within the PVsyst software. The *IV* curves for different modules were estimated using both models and compared with the measured curves to calculate their accuracy.

Figure 2a compares the Power–Voltage (*P–V*) curves estimated by the De Soto and PVsyst models with the measured *IV* curves for different illumination intensities at 25 °C. The De Soto model overestimates V_{oc} and P_{mpp} at low intensities and PVsyst overestimates them at high intensities. Figure 2b compares the model estimates with measured curves for different cell temperatures at 1000 W m^{-2} . At high temperatures, the De Soto model underestimates V_{oc} and PVsyst overestimates P_{mpp} . The *nRMSE* in estimating the maximum power point using the De Soto and PVsyst model are 26.7% and 12%, respectively (The graph representing this data is discussed later in the text).

In this work, we develop an electrical model for energy yield estimation adapting the models of significant current pathways from literature and incorporating the temperature and irradiance dependence of various parameters. These relations were determined by characterization. We also develop a step-by-step characterization strategy to obtain the parameters for using the model. The proposed characterization methods are non-destructive and can be easily done with basic PV lab instrumentation. Apart from model parameters, module temperature and incident irradiance are the only external parameters required for energy yield prediction. Thus, the proposed model can be easily combined with a thermal model and irradiance model in any of the existing energy yield prediction infrastructure. With modular and simplistic approach proposed, we ensure that the model can be used across the PV value chain. Table 1 gives the summary of the state-of-the-art models available for simulating the performance of CIGS devices and compares it with the developments made in this work.

The paper is organised as follows: The section “Proposed electrical model” explains the different components of the proposed electrical model and step-by-step characterization strategy developed to obtain the model parameters. The section “Results and discussion” presents the validation results of the model with measurements from different modules and gives recommendations on the minimal characterization data required for estimating the instantaneous power of CIGS modules.

PROPOSED ELECTRICAL MODEL

In this section, we describe the proposed models for the different current components described in the section “Introduction”. The current components can be clustered into three main

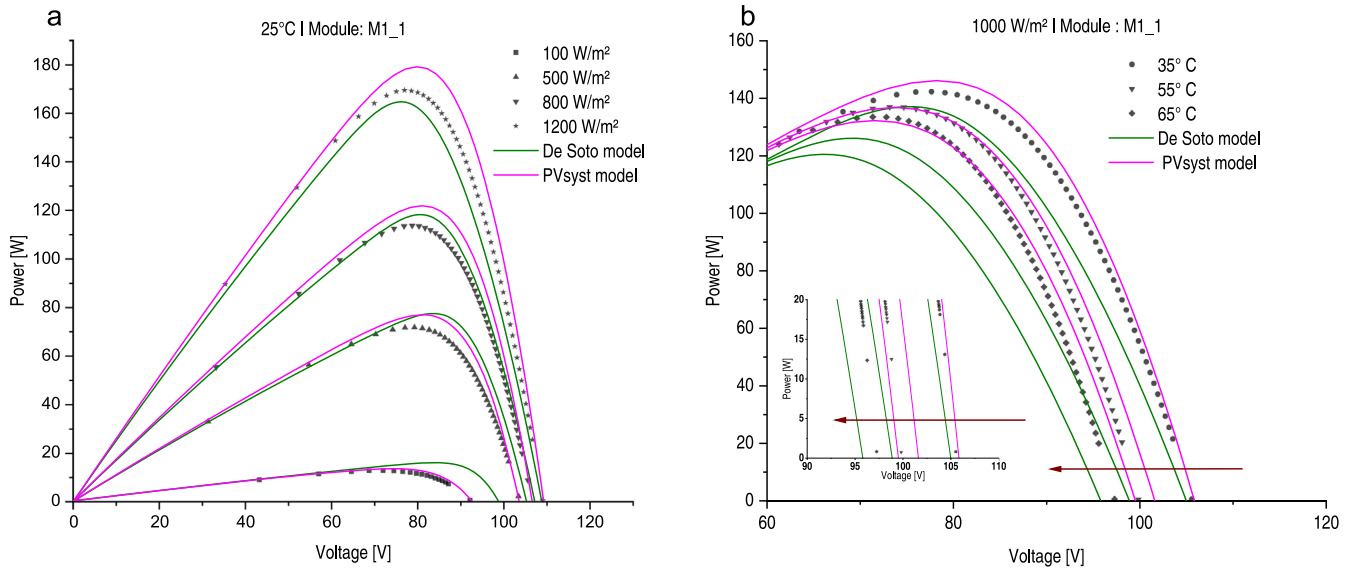


Fig. 2 Power–Voltage (P – V) characteristics estimated by the De Soto²³ and PVsyst models²¹ for a 150 Wp CIGS module compared with the measured IV curves. **a** Comparison for different irradiance intensities at 25°C. **b** Comparison of IV curves for different module temperatures at 1000 W m⁻². The markers represent the measured curves while the dotted lines show the IV curve estimation of the De Soto (green) and PVsyst models (magenta). The brown arrows indicate the order in which the PV curves are arranged (35°C, 55°C, 65°C).

Model	Physics			Parameter extraction
	Photocurrent	Shunt vs illumination	saturation current variation over illumination	
Sandia PV array performance model ¹⁶	Empirical correction factors for the combined effect			Data sheet parameters and PV performance data
Loss factor Model ²²				
De Soto ²³	Superposition assumption	Linear	Constant	Data sheet parameters
PVsyst ²¹	Superposition assumption	Exponential	Constant	Data sheet parameters and PV performance data
Sun et al. ⁶	Voltage-dependent photocurrent	Constant	Constant	Model parameters extracted through regression and numerical simulation.
This work	Voltage-dependent photocurrent	Power	Non-Linear	Parameters obtained through a simple characterization strategy developed in this work

components, photocurrent, diode current and shunt current. The below subsections explain the model for each of those components.

Photocurrent

The photocurrent model described by Sun et al.⁶ was adapted to our model as it considers voltage-dependent photogeneration and depicted in Eq. (1):

$$I_{ph}(V) = I_l \cdot \frac{1}{1 + \alpha * e^{\left(\frac{q\beta(V^* - V_{bi})}{N_s k T}\right)}} \tag{1}$$

$$V^* = V - I * R_s \tag{2}$$

The I_l is the generated photocurrent. The parameter α captures the two opposing current mechanisms at the interface: the diffusion and the thermionic emission. It is the ratio of diffusion velocity to thermionic emission velocity. β is the ratio of the electric field between the buffer and bulk layers. It is always close to 1 for CIGS cells as the thickness of the CIGS bulk is much greater than the thickness of the buffer layer. The carrier partition takes place at a

voltage equal to the built-in-voltage (V_{bi}) due to the flat conduction band. The carriers move to the opposite terminals and recombines³. This leads to a zero photocurrent at V_{bi} : $I_{ph} \approx 0$ at $V^* = V_{bi}$ for $\alpha \gg 1$ as per 2.1. V^* is the voltage that is corrected for series resistance (R_s) and given by Eq. (2). k is the Boltzmann constant and T is the temperature. N_s is the number of cells in series. The exponential part captures the zero current collection at V_{bi} .

Diode current

The dominant recombination mechanism dictates the diode current in solar cells. The three possible recombination regions in CIGS solar cells are the neutral bulk region, space charge region, and buffer-CIGS interface. Dark current further increases by tunnelling. The model described by William et al.⁹ suggests a double diode model to represent main junction recombination and a weak tunnelling junction. Since tunnelling is negligible at normal operating temperatures, we ignore the second diode. We can represent the saturation current (I_0) using a temperature-independent reference saturation current (I_{00}), activation energy (E_a) and ideality factor (n)¹¹. The value of I_{00} determines the

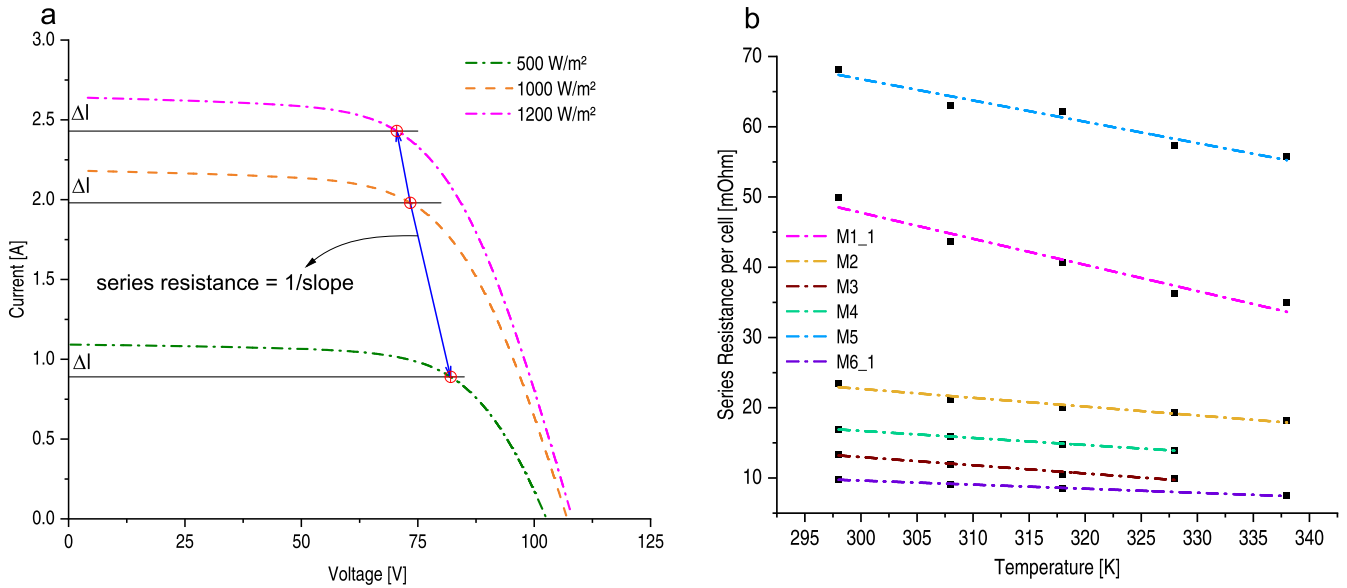


Fig. 3 Determination of series resistance and its behaviour with temperature. **a** Determining series resistance using IV curves under different illumination intensities at 25 °C. **b** Variation in series resistance of different CIGS cells with temperature. Dotted lines denote the linear fit of the data.

assumed nature of recombination in the cell¹⁰. The model for diode current is given by Eq. (3):

$$I_d(V) = I_{00} * e^{\left(\frac{-E_a}{n+N_s kT}\right)} * \left(e^{\left(\frac{qV^*}{n+N_s kT}\right)} - 1\right) \quad (3)$$

With the measurements, I_{00} was found to be dependent on illumination intensity. This is in line with the observations made by Kato et al.¹⁰.

Shunt current

Most of the reviewed models use linear and nonlinear shunt resistance (R_{sh}), when describing the shunt performance of CIGS solar cells^{6,9,14}. Here, we use a simplified Eq. (4) with only a nonlinear shunt with power factor γ :

$$I_{sh}(V) = \frac{(V^*)^\gamma}{R_{sh}}, \gamma > 1 \quad (4)$$

Current–voltage equation

With the three current components described above, the IV curve of CIGS solar cells can be represented by Eq. (5). N_p is the number of parallel strings:

$$I(V) = N_p * (I_{ph}(V) - I_d(V) - I_{sh}(V)) \quad (5)$$

Parameter estimation and their temperature and irradiance dependence

The value of parameters at standard test condition (also denoted in symbols with subscript “ref”) of 1000 W m⁻² and 25 °C serve as an input to the model. The estimation of the value for physical parameters such as series resistance (R_s), shunt resistance (R_{sh}), activation energy (E_a), saturation current (I_0) and their variation with irradiance and temperature are determined through characterization. Other parameters such as built-in-voltage (V_{bi}) and non-physical parameters such as ideality factor (n), a and γ are obtained through curve fitting with least-squares method. A wide range of modules available in the market were used for validating the model. Eight modules, referred to as M1_1, M1_2, M2, M3, M4, M5, M6_1 and M6_2, were used for model validation. The power rating and type of the modules are given in Supplementary Table 1. The idea of the paper is to compare the model accuracy among

different modules and not to compare module performance. Hence, the manufacturers’ names are not disclosed. The below subsections explain the step-by-step approach used to obtain the value of parameters and determine their dependence with temperature and irradiance.

Series resistance. There are multiple ways to identify the series resistance (R_s) of PV modules. Pysch et al.²⁵ compared various techniques in terms of their accuracy and robustness. Out of the reviewed techniques, we chose to use the method²⁶ that compares IV curves under various illumination intensities at 25 °C to determine the R_s . This method was chosen because the estimated R_s is representative of a wide range of illumination intensities.

Wolf et al.²⁶ recommends using three IV curves each at different illumination intensity. Preferably a low light intensity (≤ 500 W m⁻²) curve, a STC curve ($= 1000$ W m⁻²), a higher light intensity (> 1000 W m⁻²) curve. Series resistance is calculated by identifying the change in voltage required to produce equivalent current changes (ΔI) at the three chosen intensities. ΔI is chosen such that voltage is higher than the MPP voltage (V_{mpp}). The inverse of the slope of the line $\left|\frac{\Delta V}{\Delta I}\right|$ joining those voltage points gives the series resistance of the module. Figure 3a depicts the procedure for module M1_1 at 25 °C. Assuming all cells to have the same resistance, single cell series resistance can be determined by multiplying the factor $\frac{N_p}{N_s}$ (based on equivalent resistance of series /parallel resistor network) to the module resistance. The measurement is repeated at multiple temperatures to obtain the linear relation of the series resistance and temperature. Figure 3b shows the linear variation in R_s with temperature for different CIGS modules. The measurements were used to obtain the temperature coefficient of series resistance β_{rs} . Using the series resistance ($R_{s,ref}$) at reference temperature (T_{ref}) of 25 °C and β_{rs} , the R_s at different temperatures can be determined using Eq. (6). The variation of R_s with temperature is significant. The referred state-of-the-art models do not consider the temperature dependence of R_s .

$$R_s = R_{s,ref} + \beta_{rs}(T - T_{ref}) \quad (6)$$

Shunt resistance. Shunt resistance (R_{sh}) can be determined as the inverse slope of the IV curve at I_{sc} ($V = 0$)²⁷. Assuming same shunt

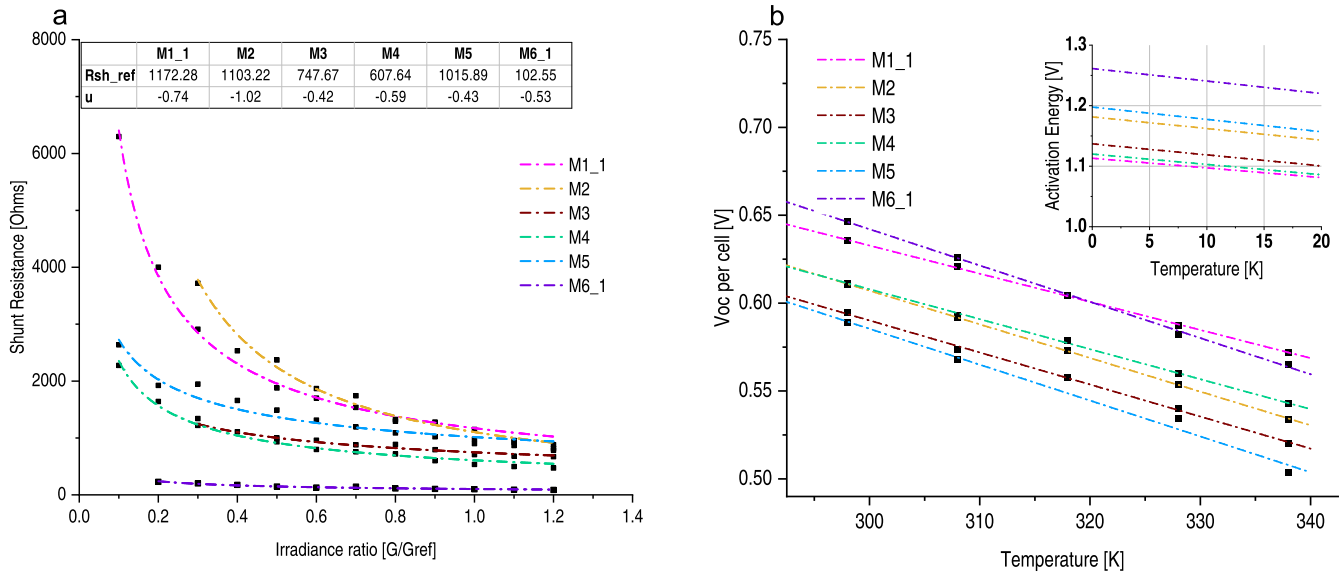


Fig. 4 Determining the shunt behaviour with irradiance and activation energy. **a** Variation of shunt resistance with irradiance for different modules. The dotted lines show the power relation fit for each of the modules. The inset table shows $R_{sh,ref}$ and fit parameter u for each of the modules. **b** variation of V_{oc} with temperature (T) for the different modules. The inset: The intercept of the V_{oc} vs. T line at 0 K representing E_a . (V_{oc} of the modules are divided by the number of cells in series to obtain the V_{oc} of the cell).

resistance for all cells, single cell shunt resistance can be obtained by multiplying the $\frac{N_s}{N_p}$ to the module shunt resistance. The measurement of shunt resistance at different incidence irradiance shows that it varies non-linearly with irradiance. We propose to use Eq. (7) to represent the shunt resistance variation for CIGS technology. $R_{sh,ref}$ is the shunt resistance at reference irradiance (G_{ref}) of 1000 W m^{-2} and G is the incident irradiance:

$$R_{sh} = R_{sh,ref} * \left(\frac{G}{G_{ref}} \right)^u \quad (7)$$

Figure 4a shows the irradiance dependence of shunt resistance for different CIGS modules. The power relation (7) was used to fit the data for each module to obtain the empirical parameter u that defines the relation. The values extracted from the data are given in inset table of Fig. 4a.

Activation energy. The activation energy (E_a) of CIGS solar cells can be obtained from the linearized temperature (T) dependence of V_{oc} ¹¹. The intercept of the line at the y-axis is the activation energy. Figure 4b shows the estimation of E_a for different modules under study. E_a (intercept) can also be estimated by considering the temperature coefficient (β_{voc}) as the slope and V_{oc} at 25 °C as a point on the line.

Ideality factor and saturation current pre-factor. The ideality factor (n) and dark saturation current pre-factor (I_{00}) can be estimated from the I_{sc} vs. V_{oc} curve obtained by plotting I_{sc} vs. V_{oc} (cell parameters) at different irradiance intensities. This method is used with an assumption that at V_{oc} , diode current is equal to photocurrent and shunt current is negligible. However, our model considers voltage-dependent photogeneration, illumination-dependent dark saturation current, and non-negligible shunt current. The value of n and I_{00} cannot be directly used as the reference parameters. Equation (8) was used to fit the I_{sc} vs. V_{oc} to get an initial estimate for n and I_{00} .

$$I_{sc} = I_{00} * e^{\left(\frac{-E_g + q}{n * kT} \right)} * e^{\left(\frac{V_{oc} + q}{n * kT} \right)} \quad (8)$$

Curve fitting. At this point, the reference values $R_{s,ref}$, E_a , and $R_{sh,ref}$ (cell parameters) have been estimated. Now, the IV curve at STC can be fitted to the Eq. (5) using python SciPy curve fit

function²⁸ to obtain the remaining parameters α_{ref} , $V_{bi,ref}$, n , $I_{00,ref}$, and γ_{ref} . Equations (9) and (10), adapted from⁵ give the temperature relation of the parameters α and V_{bi} , respectively. Here ΔE_c refers to the conduction band offset between the buffer and absorber. Value of $\Delta E_c = 0.1 \text{ eV}$ fits well for the CIGS technology. For some modules, γ exhibited slight temperature dependence given by Eq. (11), where m is either 0 or 1:

$$\alpha = \alpha_{ref} * e^{\frac{\Delta E_c + q}{k} * \left(\frac{1}{T_{ref}} - \frac{1}{T} \right)} \quad (9)$$

$$V_{bi} = \Delta E_c + E_{g,ref} + \frac{T_{ref}}{T} * (V_{bi,ref} - \Delta E_c - E_{g,ref}) - k * T_{ref} * \ln \left(\frac{T}{T_{ref}} \right) \quad (10)$$

$$\gamma = \gamma_{ref} * \left(\frac{T_{ref}}{T} \right)^m \quad (11)$$

Irradiance dependence of saturation current. After estimating all the parameters at STC, I_{00} can be estimated at different irradiance conditions using I_{sc} and V_{oc} values at different irradiance levels. I_{00} was found to have a power dependence on irradiance. We arrived at the expression (12) by obtaining I_{00} at the different irradiances. The curve was then fitted with the expression to obtain the empirical factor b . Figure 5 shows the fit for different modules.

$$I_{00} = I_{00,ref} * \left(\frac{G}{G_{ref}} \right)^b \quad (12)$$

RESULTS AND DISCUSSION

Having estimated all the required parameters using the above proposed methodology, IV curves for a wide range of operating conditions were simulated using the model. The section "Accuracy" compares the simulated IV curves with the respective measured IV curves and establishes the accuracy of the model across different operating conditions. The section "Statistical significance" discusses the statistical significance of the model using t test.

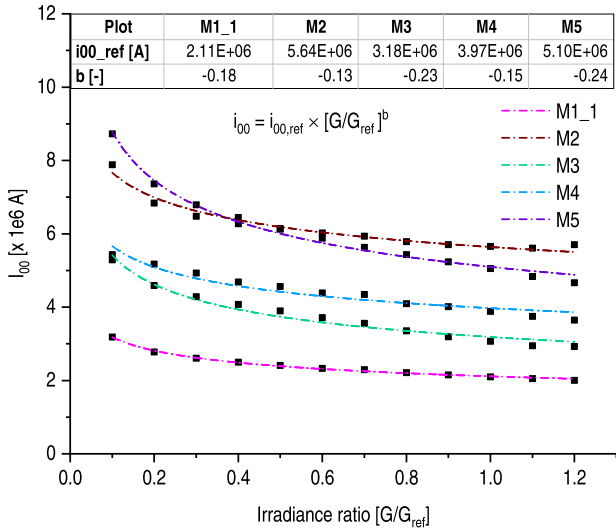


Fig. 5 Variation of I_{00} with illumination for five module samples. Fitting is used to obtain the power factors. The inset table shows the results of the fit.

Accuracy

Figure 6 visualizes the measured and simulated IV curves for two of the module samples. The markers represent the measured curves for different temperatures and irradiances while the dotted lines represent the IV curves estimated by the model. We refer the readers to Supplementary Figs. 1–6 for the IV curve estimation of other samples.

The accuracy of the model is quantified in terms of P_{mpp} . Figure 7a shows the descriptive statistics of the estimation error at different irradiances. Figure 7b, in turn, shows the power estimation error at different operating temperatures. The power estimation error is well within the 5% range at all the considered operating conditions. The variation in the median error is small and does not show any trend with irradiance or temperature. This proves that the model does not have a bias towards any set of operating conditions. Figure 8 compares the power estimation error of the developed model with the existing state of the art: the De Soto and PVSyst models. $nRMSE$ and $nMBE$ are computed for the models and are quoted in the inset table in Fig. 8. The $nRMSE$ and $nMBE$ of the proposed model are significantly lower than the other state-of-the-art models.

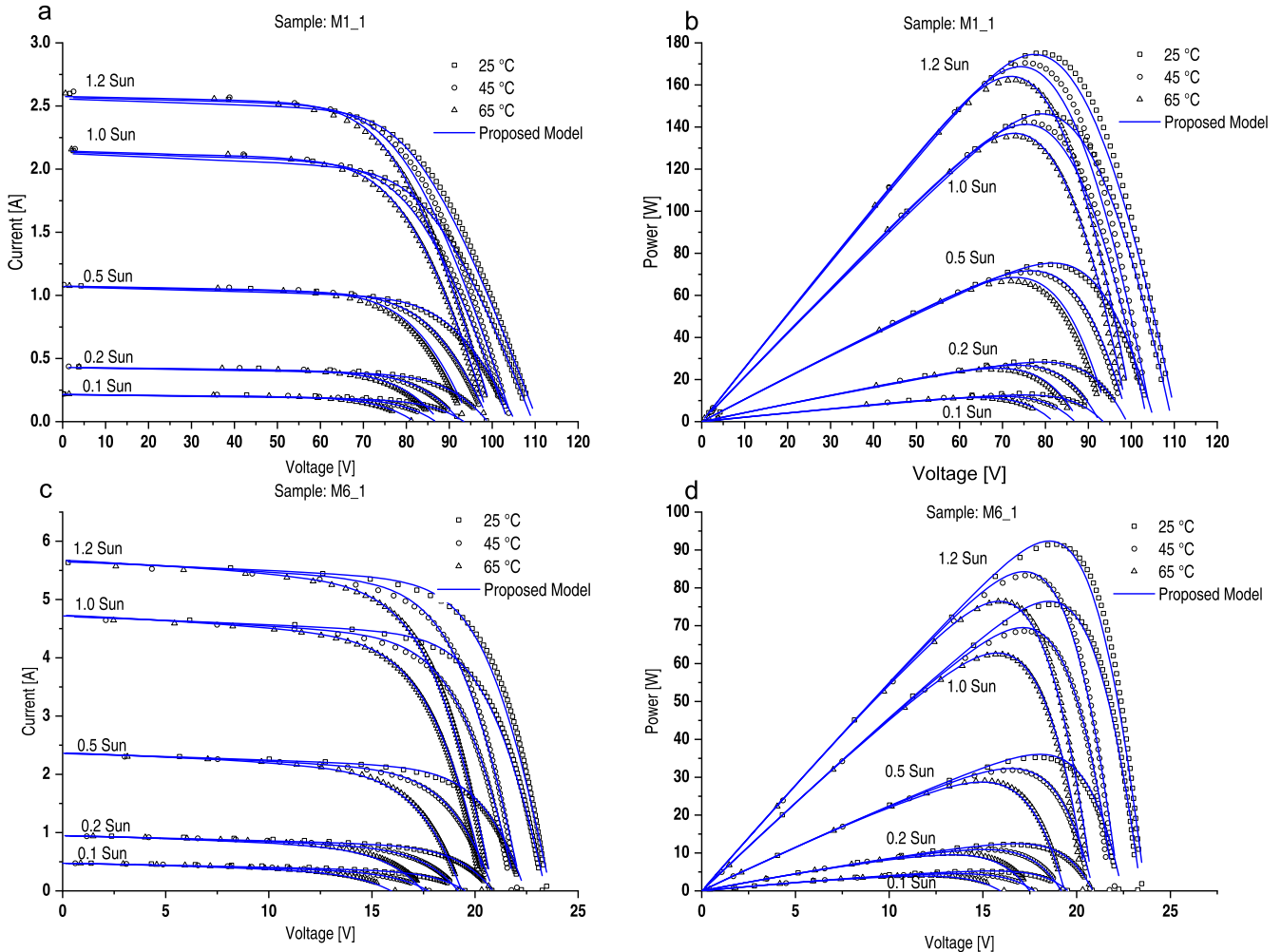


Fig. 6 Simulated and measured IV and $P-V$ curves for module samples $M1_1$ and $M6_1$. The markers represent the measured IV points, and the blue lines represent the IV curves estimated by the developed model.

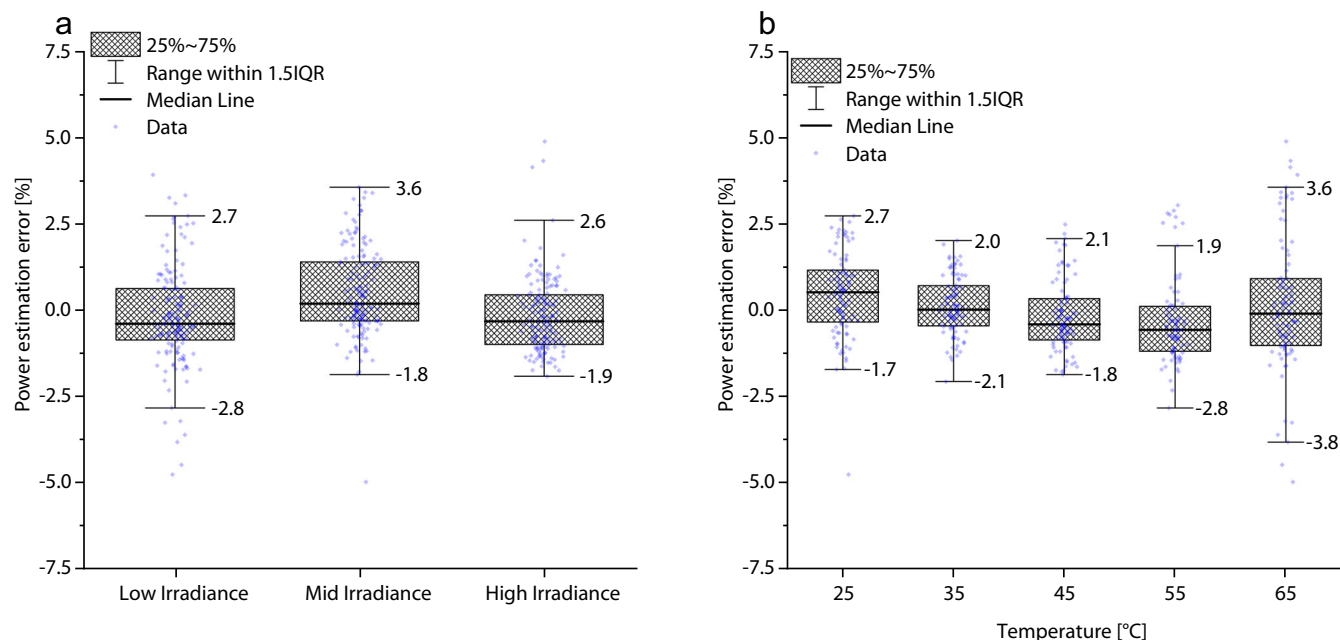


Fig. 7 Descriptive statistics of power estimation error. Statistical analysis of the model error across (a) different irradiance regions and (b) temperatures. ‘Low Irradiance’, ‘Mid Irradiance’ and ‘High Irradiance’ represent the operating points within the ranges between 100 W m^{-2} and 400 W m^{-2} , 500 W m^{-2} and 800 W m^{-2} , and 900 W m^{-2} and 1200 W m^{-2} , respectively. The checked boxes show the middle 50% of the data points (i.e., the range between the 25th and 75th percentile). The whiskers represent data points outside the middle 50% and within 1.5 times the interquartile range (IQR).

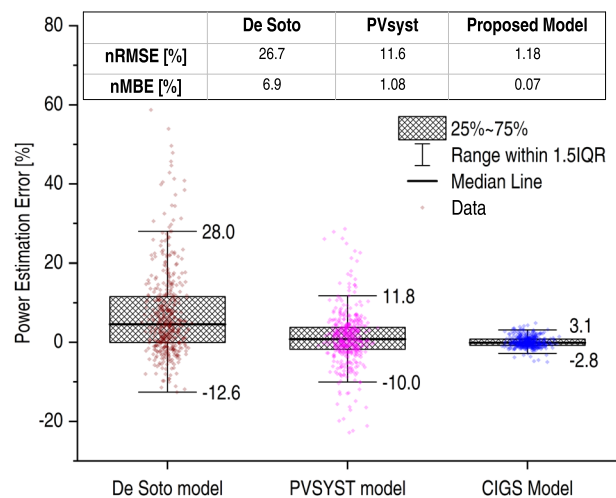


Fig. 8 Comparison of accuracy of the developed model (blue) with that of the De Soto (brown) and PVsyst (magenta) models. The graph contains error estimates of all considered operating points in the ranges of $25 \text{ }^{\circ}\text{C}$ to $65 \text{ }^{\circ}\text{C}$ and 100 W m^{-2} to 1200 W m^{-2} for eight CIGS modules. The checked boxes show the middle 50% of the data points (i.e., the range between the 25th and 75th percentile). The whiskers represent data points outside the middle 50% and within 1.5 times the interquartile range (IQR). The inset table shows the nRMSE and nMBE error for each of the model.

Statistical significance

The independent sample t-test was used to analyse the statistical significance of the derived error metrics. The assumed null hypothesis is that the mean error is zero, while the alternative hypothesis is that the mean error significantly differs from zero. The assumed significance level is 5%. The result of the hypothesis testing is shown in Table 2.

Table 2. Results of the hypothesis testing for the error metrics of each model.

Parameter	De Soto	PVsyst	This work
No. of samples	465	465	465
Mean [%]	6.62	1.09	0.07
Standard deviation [%]	10.81	6.54	1.33
Significance level	0.05	0.05	0.05
t statistic	13.80	3.58	1.14
p-value	$1.50\text{e}-36$	$3.73\text{e}-4$	0.26
Null hypothesis	Rejected	Rejected	Not rejected

For the De Soto and PVsyst models, the p-value is much less than the significance level. Thus, the null hypothesis is rejected, which means the mean error significantly differs from the test mean, 0. The null hypothesis holds for the developed model, which means that the mean error does not significantly differ from the test mean, 0. This proves that the developed model has statistically significant accuracy compared to the other models. This validates the model. Suitability of the model to represent other thin-film technologies like ultra-thin CIGS and Cadmium telluride (CdTe) are discussed in section Supplementary Discussions.

Minimal characterization requirement

In this section, the minimal characterization data required to estimate the value of parameters are discussed and compared with the characterization requirement standardized under IEC 61853.

Series resistance and activation energy. As discussed in the section ‘‘Parameter estimation and their temperature and irradiance dependence’’, IV curves at 1000 W m^{-2} , at an illumination intensity above 1000 W m^{-2} , and at an illumination intensity of around 500 W m^{-2} are required to extract series resistance.

Table 3. *IV* curves required as per IEC 61853-1 (marked as IEC) and the *IV* curves required for using the proposed model (marked as PM).

		Incident Irradiance [W m^{-2}]											
		100	200	300	400	500	600	700	800	1000	1100	1200	
Temperature [$^{\circ}\text{C}$]	15	IEC	IEC	IEC	IEC	IEC	IEC	IEC	IEC	IEC	IEC	IEC	IEC
	25	IEC	PM	IEC	PM	IEC	PM	IEC	PM	IEC	PM	IEC	PM
	45					PM				PM			PM
	50				IEC			IEC		IEC		IEC	
	65					PM				PM			PM
	75							IEC		IEC		IEC	

To measure its temperature coefficient, the three *IV* curves must be measured at, at least three different temperatures as wide as possible. V_{oc} obtained at different temperature can be used to measure the activation energy.

Shunt resistance, ideality factor, and saturation current pre-factor. To measure shunt resistance and its illumination intensity dependence, at least six *IV* curves at different illumination intensities (at 25 $^{\circ}\text{C}$) are required. The low-intensity curves are preferred for the better estimation of the parameter u . Ideality factor, saturation current pre-factor, and irradiance dependence of shunt resistance can also be derived from the I_{sc} and V_{oc} values obtained from the *IV* curves at different illumination intensities (at 25 $^{\circ}\text{C}$).

The IEC 61853 standard²⁹ requires the power to be measured at 21 sets of operating conditions shown in Table 3. From the above discussion, we can establish that the *IV* curves measured at 12 sets of operating conditions are sufficient for estimating the performance of CIGS solar cells across a wide range of operating conditions. The recommended operating points shown in Table 3 is based on the qualitative discussion made above. To establish the gain or loss in accuracy due to the inclusion of specific data point or due to the difference in number of required input data points is in itself a separate study and out of the scope of this paper. Table 3 acts as a mere guideline to use the model. The IEC 60891 defines three procedures to translate a curve measured at an operating condition to any other operating condition. The developed model also acts as a translation procedure specific to the CIGS technology. New CIGS-specific IEC standards could be established based on this work.

In conclusion, an electrical model with temperature and irradiance dependencies of different current components was developed to represent CIGS PV technology. A detailed characterization strategy was developed to obtain the value of model parameters. The model has $nMBE$ of $\sim 0\%$ and $nRMSE$ of 1.2%, which is significantly lower than state-of-the-art models. Thus, the proposed electrical model can be used to estimate energy yield with higher accuracy than the existing models and can be easily integrated into any existing energy yield prediction systems. This electrical model is the first step in our goal to create a simulation infrastructure for thin-film PV technologies. Our research work will move towards perovskites and then towards tandem architectures with an additional focus on integrated PV.

METHODS

The Wavelabs Sinus 2100³⁰ setup at IMEC/EnergyVille, Genk was used to characterize the PV modules. The simulator ensures A+++ level of temporal spectral stability. The built-in spectrometer can be used to calibrate the spectral accuracy and intensity. The temperature controller in the setup enables us to characterize the modules at operating temperatures between 15 $^{\circ}\text{C}$ and 65 $^{\circ}\text{C}$. Five calibrated temperature sensors were used to measure the temperature at the backsheet or the rear glass of the module. The modules were thermally-soaked to ensure that a steady state has been reached.

DATA AVAILABILITY

The datasets generated and analysed during the study are available from the corresponding author on reasonable request.

Received: 4 March 2022; Accepted: 13 October 2022;

Published online: 27 October 2022

REFERENCES

- Philippis, S. & Warmuth, W. *Photovoltaics Report—Fraunhofer ISE*. <https://www.ise.fraunhofer.de/conten%0Ant/dam/ise/de/documents/publications/studies/Photovoltaics-Report.pdf> (2020).
- Corti, P., Bonomo, P., Frontini, F., Macé, P. & Bosch, E. *Building Integrated Photovoltaics: A Practical Handbook For Solar Buildings' Stakeholders Status Report*. <http://repository.supsi.ch/id/eprint/12186> (2020).
- Moore, J. E., Dongaonkar, S., Chavali, R. V. K., Alam, M. A. & Lundstrom, M. S. Correlation of built-in potential and I-V crossover in thin-film solar cells. *IEEE J. Photovolt.* **4**, 1138–1148 (2014).
- Gloeckler, M., Jenkins, C. R. & Sites, J. R. Explanation of light/dark superposition failure in CIGS solar cells. *Mater. Res. Soc. Symp. Proc.* **763**, 231–236 (2003).
- Chavali, R. V. K., Wilcox, J. R., Ray, B., Gray, J. L. & Alam, M. A. Correlated nonideal effects of dark and light I-V characteristics in a-Si/c-Si heterojunction solar cells. *IEEE J. Photovolt.* **4**, 763–771 (2014).
- Sun, X., Silverman, T., Garris, R., Deline, C. & Alam, M. A. An Illumination- and Temperature-Dependent Analytical Model for Copper Indium Gallium Diselenide (CIGS) Solar Cells. *IEEE J. Photovolt.* **6**, 1298–1307 (2016).
- Hegeedus, S., Desai, D. & Thompson, C. Voltage dependent photocurrent collection in CdTe/CdS solar cells. *Prog. Photovolt.* **15**, 587–602 (2007).
- Liu, X. X. & Sites, J. R. Solar-cell collection efficiency and its variation with voltage. *J. Appl. Phys.* **75**, 577–581 (1994).
- Williams, B. L. et al. Identifying parasitic current pathways in CIGS solar cells by modelling dark J-V response. *Prog. Photovolt.* **23**, 1516–1525 (2015).
- Kato, T., Tai, K. F., Yagioka, T., Kamada, R. & Sugimoto, H. Recombination analysis of CIGS solar cells using temperature and illumination dependent open-circuit voltage measurement. In: *International Photovoltaic Science and Engineering Conference* 1–4. https://www.researchgate.net/publication/327972450_Recombination_analysis_of_CIGS_solar_cells_using_temperature_and_illumination_dependent_opencircuit_voltage_measurement (2016).
- Rau, U. & Schock, H. W. Electronic properties of Cu(In,Ga)Se₂ heterojunction solar cells—recent achievements, current understanding, and future challenges. *Appl. Phys. A* **69**, 131–147 (1999).
- Zelenina, A., Werner, F., Elanzeery, H., Melchiorre, M. & Siebentritt, S. Space-charge-limited currents in CIS-based solar cells. *Appl. Phys. Lett.* **111**, 213903 (2017).
- Dongaonkar, S. et al. Universal statistics of parasitic shunt formation in solar cells, and its implications for cell to module efficiency gap. *Energy Environ. Sci.* **6**, 782–787 (2013).
- Dongaonkar, S. et al. Universality of non-Ohmic shunt leakage in thin-film solar cells. *J. Appl. Phys.* **108**, 124509 (2010).
- Liao, Y., Kuo, S., Hsieh, M., Lai, F. & Kao, M. A look into the origin of shunt leakage current of Cu (In, Ga) Se 2 solar cells via experimental and simulation methods. *Sol. Energy Mater. Sol. Cells* **117**, 145–151 (2013).
- King, D. L., Boyson, W. E. & Kratochvil, J. A. Photovoltaic Array Performance Model, *SANDIA Report SAND2004-3535* Sandia National Laboratories (2004).
- Farias Basulto, F. & Guillermo, A. *CIGSse Thin Film Photovoltaic Yield Improvement for Operating Conditions* (Technical University Berlin, 2021). <https://doi.org/10.14279/depositonce-12576>.

18. Louwen, A., Schropp, R. E. I., van Sark, W. G. J. H. M. & Faaij, A. P. C. Geospatial analysis of the energy yield and environmental footprint of different photovoltaic module technologies. *Sol. Energy* **155**, 1339–1353 (2017).
19. Blair, N. et al. *System Advisor Model (SAM) General Description* (OSTI.GOV, 2018).
20. Holmgren, W. F., Hansen, C. & Mikofski, M. A. pvlib python: a python package for modeling solar energy systems. *J. Open Source Softw.* **3**, 884 (2018).
21. Sauer, K. J., Roessler, T. & Hansen, C. W. Modeling the irradiance and temperature dependence of photovoltaic modules in PVsyst. *IEEE J. Photovolt.* **5**, 152–158 (2015).
22. Sellner, S., Sutterluti, J., Schreier, L. & Ransome, S. Advanced PV module performance characterization and validation using the novel Loss Factors Model. In: *2012 38th IEEE Photovoltaic Specialists Conference* 002938–002943 (IEEE, 2012). <https://doi.org/10.1109/PVSC.2012.6318201>.
23. de Soto, W., Klein, S. A. & Beckman, W. A. Improvement and validation of a model for photovoltaic array performance. *Sol. Energy* **80**, 78–88 (2006).
24. Laudani, A., Riganti Fulginei, F. & Salvini, A. Identification of the one-diode model for photovoltaic modules from datasheet values. *Sol. Energy* **108**, 432–446 (2014).
25. Pysch, D., Mette, A. & Glunz, S. W. A review and comparison of different methods to determine the series resistance of solar cells. *Sol. Energy Mater. Sol. Cells* **91**, 1698–1706 (2007).
26. Wolf, M. & Rauschenbach, H. Series resistance effects on solar cell measurements. *Adv. Energy Convers.* **3**, 455–479 (1963).
27. Diantoro, M. et al. Shockley's equation Fit analyses for solar cell parameters from I-V curves. *Int. J. Photoenergy* **2018**, 1–7 (2018).
28. Virtanen, P. et al. SciPy 1.0: fundamental algorithms for scientific computing in Python. *Nat. Methods* **17**, 261–272 (2020).
29. IEC 61853-1 *Photovoltaic (PV) Module Performance Testing and Energy Rating—Part 1: Irradiance and Temperature Performance Measurements and Power Rating* (International Standard, 2011).
30. Wavelabs-SINUS-2100. *Wavelabs* <https://wavelabs.de/products/sinus-2100-parachute/>.

ACKNOWLEDGEMENTS

The work is supported by the Kuwait Foundation for the Advancement of Sciences (KFAS) under project number CN18-15EE-01 and by Flanders Innovation & Entrepreneurship and Flux50 under project DAPPER, HBC.2020.2144.

AUTHOR CONTRIBUTIONS

S.R. developed the model, characterized the PV modules, validated the model with measurements and wrote the paper. A.T. supervised the model development, verified

the results, and contributed significantly to review the draft versions of this paper. A.H. made the statistical analysis of the results and reviewed the draft versions of this paper. M.M. helped acquire module samples and reviewed this paper. B.V. helped to acquire module samples from industrial partners, advised with the technical expertise, verified the results, and reviewed the draft version of this paper. J.P. supervised the entire work, advised with the technical expertise, verified the results, and reviewed the draft versions of this paper.

COMPETING INTERESTS

The authors declare no competing interests.

ADDITIONAL INFORMATION

Supplementary information The online version contains supplementary material available at <https://doi.org/10.1038/s41528-022-00220-5>.

Correspondence and requests for materials should be addressed to Santhosh Ramesh.

Reprints and permission information is available at <http://www.nature.com/reprints>

Publisher's note Springer Nature remains neutral with regard to jurisdictional claims in published maps and institutional affiliations.



Open Access This article is licensed under a Creative Commons Attribution 4.0 International License, which permits use, sharing, adaptation, distribution and reproduction in any medium or format, as long as you give appropriate credit to the original author(s) and the source, provide a link to the Creative Commons license, and indicate if changes were made. The images or other third party material in this article are included in the article's Creative Commons license, unless indicated otherwise in a credit line to the material. If material is not included in the article's Creative Commons license and your intended use is not permitted by statutory regulation or exceeds the permitted use, you will need to obtain permission directly from the copyright holder. To view a copy of this license, visit <http://creativecommons.org/licenses/by/4.0/>.

© The Author(s) 2022